

Short Communication

Corrosion Behaviour of Electroless Deposited Ni–P/BN(h) Composite Coating

Chih-I Hsu¹, Gao-Liang Wang^{2,*}, Ming-Der Ger³, Kung-Hsu Hou^{4,*}

¹School of Defense Science, Chung Cheng Institute of Technology, National Defense University, Taoyuan, Taiwan

²Department of Marketing Management, Takming University of Science and Technology, Taipei, Taiwan

³Department of Chemistry and Material Engineering, Chung Cheng Institute of Technology, National Defense University, Taoyuan, Taiwan

⁴Department of Power Vehicle and Systems Engineering, Chung Cheng Institute of Technology, National Defense University, Taoyuan, Taiwan

*E-mail: khou@ndu.edu.tw, khoucloud@gmail.com, wanggl@takming.edu.tw

Received: 14 February 2016 / Accepted: 29 March 2016 / Published: 4 May 2016

In this study, self-lubrication BN(h) particles successfully co-deposited on Ni–P coating through electroless deposition process, and conduct research for the Ni–P/BN(h) composite coating surface morphology, microstructure, mechanical properties and corrosion behaviour. Scanning electron microscopy (SEM) and atomic force microscope (AFM) were used to observe the micro morphology of coating, and X-ray diffraction (XRD) to analyse crystalline phase. The corrosion resistance was evaluated through polarization curves and electrochemical impedance spectroscopy (EIS) in 3.5 wt.% NaCl solution at room temperature. The results show that the hardness of Ni–P/BN(h) composite coating can be improved after heat treatment. According to the results of corrosion testing in the 3.5 wt.% NaCl solution, the corrosion resistance of electroless Ni–P/BN(h) composite coatings has been strengthened due to barrier effect by BN(h) particles, compared to a conventional Ni–P coating.

Keywords: Electroless, Ni–P/BN(h) Composite coating, Mechanical properties, Corrosion resistance

1. INTRODUCTION

Corrosion and wear are the most common reasons of degradation in mechanical parts. Hence, related researches have been conducted to develop effective methods of corrosion and wear prevention. In the past studies, electroless coating processing is a significant method to enhance the corrosion and wear resistance which is not restricted by the parts shape[1].

In the modern industrial applications, electroless Ni–P composite coatings have been widely used in many application areas for the particular properties such as corrosion resistance, wear resistance, non-magnetism, improved hardness and coating thickness uniformity[2; 3]. To choose suitable particulate materials can easily produce functional composite coatings with highly specific characteristics. These solid particles such as diamond, PTFE, B₄C, MoS₂, SiO₂, SiC or Al₂O₃ can be usually chosen to improve corrosion and wear behaviors [4-20]. These applications in various industries provide components with higher quality and longer lifetime.

Among the particulate materials used for self-lubricating, boron nitride of hexagonal close-packed structure BN(h) has excellent electrical insulation, thermal conductivity, oxidation resistance and good chemical stability. Therefore, it is an excellent solid lubricant often interested in the industry, and is frequently studied and applied in various industries[21]; According to literature, the addition of the BN(h) can improve the wear properties [22-25] of nickel matrix composite coatings. However, there are no reports regarding the corrosion resistance mechanism of the BN(h) strengthened nickel composite coatings.

In this paper, the effects on mechanical properties and corrosion behavior of submicron BN(h) particles co-deposited on Ni–P matrix have been investigated, while compared with Ni–P coating and iron substrate.

2. EXPERIMENTAL DETAILS

Ni–P and Ni–P/BN(h) composite coatings were deposited on iron substrates (50 mm×25 mm×2 mm). Prior to the coating process, the substrates were degreased with acetone, cleaned in an alkaline solution and thoroughly washed with distilled water.

Table 1. Pre-treatment steps.

Steps	
1	Ultrasonic degreasing using acetone at 25 °C for 10 min
2	Rinse in NaOH (10%) at 40 °C for 1.5 min
3	Pickling in HCl(50%) at 25 °C for 30 s

Finally, the surfaces of all the above prepared substrates were activated. Pretreatment steps are shown in Table 1. Deposition of Ni–P/BN(h) composite coatings was performed by adding a predetermined weight of BN(h) powder (0.5–0.7 μm particle size) into the bath. A suitable surfactant CTAB was added to the solution before adding BN(h) powder. This important step is not only to improve the stability of suspension by increasing the surface charge, but also to increase the wettability of suspended particles, thus preventing their agglomeration. Moreover, the presence of surfactant can increase the electrostatic adsorption of suspended particles on the substrate to achieve the uniformity

and optimum content of BN(h) particles in Ni–P matrix. Deposition parameters for electroless Ni–P/BN(h) composite coatings are shown in Table 2. Among them, the deposition thickness of each coatings are controlled in the range of 12 μ m.

Table 2. Solution composition and operating conditions for electroless plating bath.

Coating bath composition		
1	Nickel sulfate	30g/L
2	Sodium lactate	40ml/L
3	Glycine	10g/L
4	Hypophosphite	30g/L
5	KIO ₃	2ml/L
6	CO890	1ml/L
7	BN(h) Particles	0 and 10g/L
Operating Conditions		
1	pH	5.2
2	Temperature	90°C
3	Stirring speed	100rpm

The chemical composition of the synthesized coatings was determined with Electron probe micro-analyzer (EPMA) analyses. The phase and structural analysis of the coatings were carried out using X-ray diffractometer (XRD) equipped with Cu Ka radiations. The surface morphology of the coatings was determined with the help of scanning electron microscope (SEM) and atomic force microscopy (AFM).

The electroless Ni–P and Ni–P/BN(h) composite coatings were heat treated in a tube furnace under vacuum atmosphere at 400°C for 1h. The hardness of the coatings was measured with a Vickers micro hardness indenter with a load of 50g for 10s, the hardness results were obtained from the average of 5 measurements.

Polarization test was carried out using a conventional three-electrode system. The auxiliary electrode was a platinum foil, the reference electrode was a standard calomel electrode (SCE), and the samples with an exposed area of 1.76 cm² as working electrode. The test was performed with scan rate of 0.5mVs⁻¹ by using potentiostat in 3.5 wt.% NaCl solution. Corrosion potentials and corrosion current densities were extracted from the plots using Tafel extrapolation method. The Electrochemical impedance spectroscopy(EIS) measurements were performed for corrosion potential at sinusoidal voltage excitation with perturbation amplitude of 10 mV in a frequency range from 100 kHz to 0.01 Hz. All of the impedance values were recorded and displayed as Nyquist.

3. RESULTS AND DISCUSSION

3.1. Coating morphology

Figure 1 shows the cross-section images of Ni–P and Ni–P/BN(h) composite coatings. The BN(h) particles are visible as small black spots that have been uniformly distributed throughout the Ni–P matrix. Particles can be evenly deposited in coating that the critical factors is the surface potential of BN(h) particles have been changed the nature by CTAB surfactant, so that the particles can completely suspension in the bath, and is successfully covered in the Ni–P matrix.

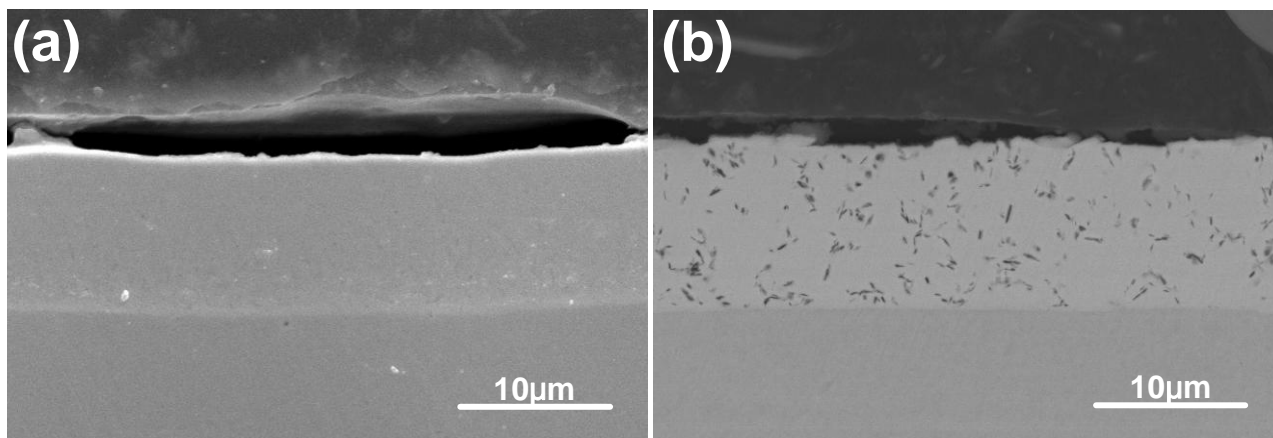


Figure 1. SEM images of the cross section of (a) Ni–P and Ni–P/BN(h) composite coatings.

Table 3 presents the chemical composition of Ni–P and Ni–P/BN(h) composite coatings. It can be noticed that BN(h) content in the Ni–P matrix can reach 2.66wt%, and phosphorus content have slightly decreased with respect to Ni–P coating. Similar studies have been explored in [5; 9; 14; 26; 27].

Table 3. Chemical compositions of Ni–P and Ni–P/BN(h) composite coatings.

Coatings	Ni (wt%)	P (wt%)	BN(h) (wt%)
Ni–P	88.18	11.82	—
Ni–P/BN(h)	89.67	7.67	2.66

The AFM images obtained from the surface of the Ni–P and Ni–P/BN(h) composite coatings are shown in Figure 2. By comparing the surface roughness profiles of both coatings, it can be noticed the surface of Ni–P coatings is quite smooth with average surface roughness of 13.9 nm. However, the surface roughness of Ni–P/BN(h) composite coatings is 21.7 nm compared to Ni–P coatings which is relatively rougher. This result indicates that incorporation of BN(h) particles into Ni–P matrix has resulted in relatively high surface roughness. Shakoor [28] et al. study Al₂O₃ particles co-deposited into Ni–B matrix which result in higher roughness compare with Ni–B coatings.

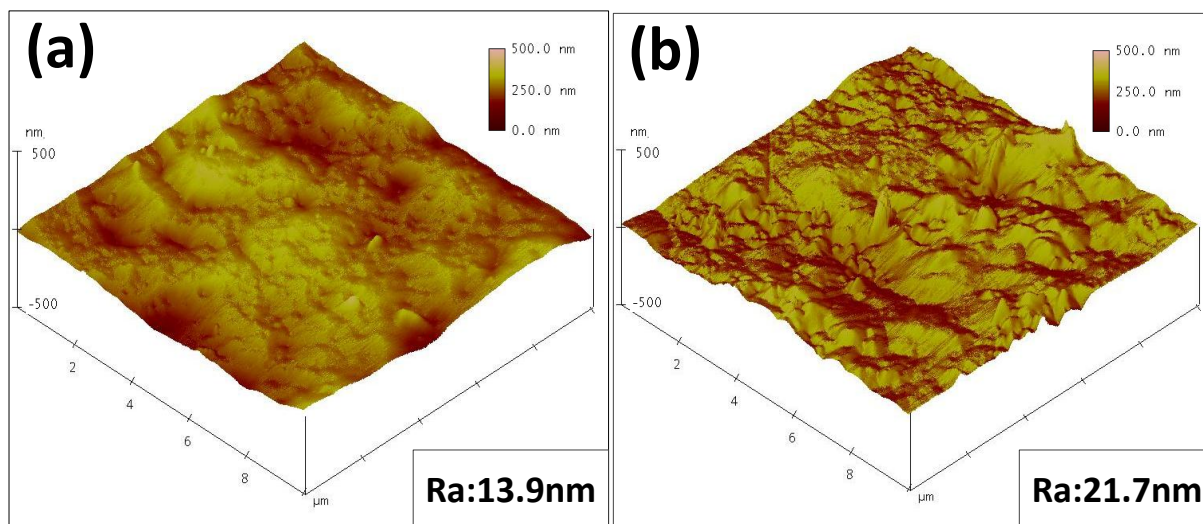


Figure 2. AFM images of the surface morphology of (a) Ni–P and Ni–P/BN(h) composite coatings.

3.2. Microstructural analysis

The X-ray diffraction patterns of the Ni–P coating in as-plated and heat treated conditions are shown in Figure 3a.

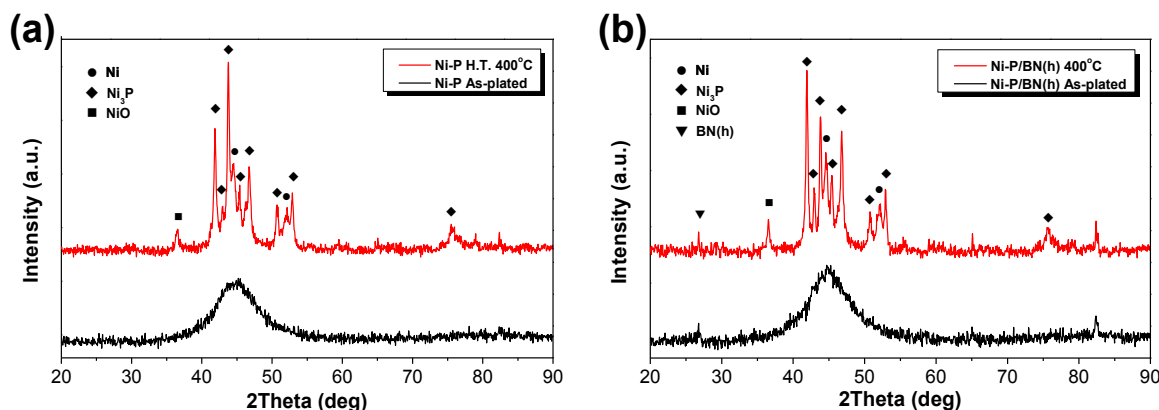


Figure 3. The XRD patterns of (a) Ni–P and (b) Ni–P/BN(h) composite coatings.

It is observed that the as-plated coatings had amorphous microstructure and exhibited a single broad peak centered at 44.5° , and changed into crystalline form after heat treatment reached 400°C for 1 hour, as a result of transformation of Ni–P matrix to the system comprising Ni and Ni_3P . This indicates that the crystallization of Ni and Ni_3P is created from the amorphous Ni–P phase. These results agree with the studies of investigators reporting that the formation of the Ni_3P phase started at 400°C treatment[9; 29].

The X-ray diffraction patterns of the Ni–P/BN(h) composite coating in as-plated and heat treated conditions are shown in Figure 3b. It shows that the microstructure of Ni–P/BN(h) composite coating in the range of 2θ angles is similar to Ni–P coating. The XRD pattern comparison also

confirms that the crystal structure of Ni–P matrix did not change after incorporation of BN(h) particles. Similar observation has been made by Mazaheri et al. [5]. However, BN(h) particles are added so that BN(h) diffraction peaks can be seen in their XRD patterns, while also confirmed the presence of the BN(h) particles embedded into the nickel matrix[9].

3.3. Mechanical properties

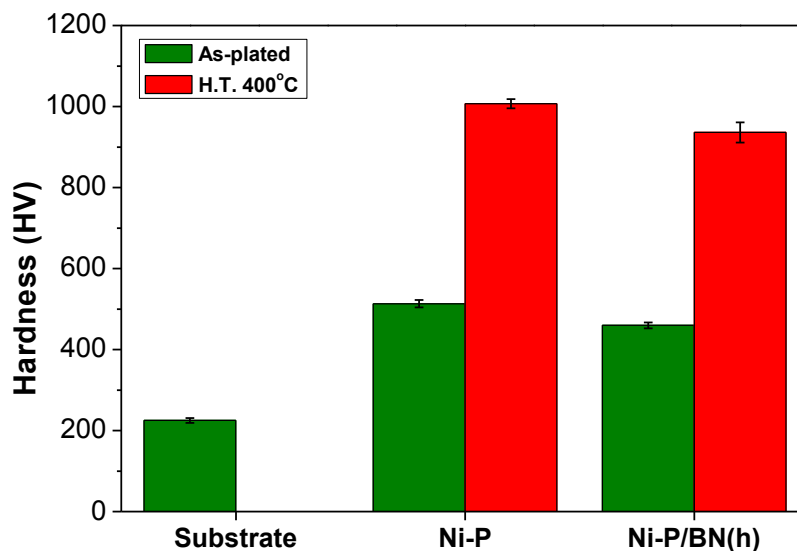


Figure 4. The effect of heat treatment on the hardness of iron substrate, Ni–P and Ni–P/BN(h) composite coatings.

Figure 4 shows the hardness of iron substrate, Ni–P and Ni–P/BN(h) composite coatings, as for comparison, their hardness are tested after heat treatment at 400°C for 1 hour. It can be seen that the hardness of iron substrate is about 225HV. After depositing the Ni–P coating, the hardness was increased to 512 HV. After adding BN(h) particles into the coating, the hardness was reduced to 463 HV. The research showed hardness is deteriorated with particles co-deposited onto nickel matrix [6; 30-34]. The BN(h) particles are a type of solid lubrication material which has a lamellar crystalline structure, in which the binding between layers is almost entirely by means of weak van der Waals forces. This structure is similar to that of graphite, which the mechanism behind their effective lubricating performance is understood to be owing to easy shearing along the basal plane of the hexagonal crystalline structures[18]. Based on this characteristic, when BN(h) particles uniformly distributed in the matrix, hardness is weakened.

After heat treatment at 400°C, the hardness of Ni–P/BN(h) composite coatings can be strengthened to 936 HV. Due to the amorphous Ni–P matrix which can be consumed to form crystallites of Ni₃P and Ni at the temperature of 400°C. The Ni₃P is formed in the ductile nickel matrix as a hard phase and markedly increases the hardness of Ni–P/BN(h) composite coatings. This phenomenon agrees with this in several reports[10; 35].

3.4. Corrosion behavior

3.4.1. Potentiodynamic polarization

Potentiodynamic polarization curves for iron substrate, Ni-P and Ni-P/BN(h) composite coatings are shown in Figure 5. The electrochemical corrosion parameters derived from the potentiodynamic polarization curves are tabulated in Table 4.

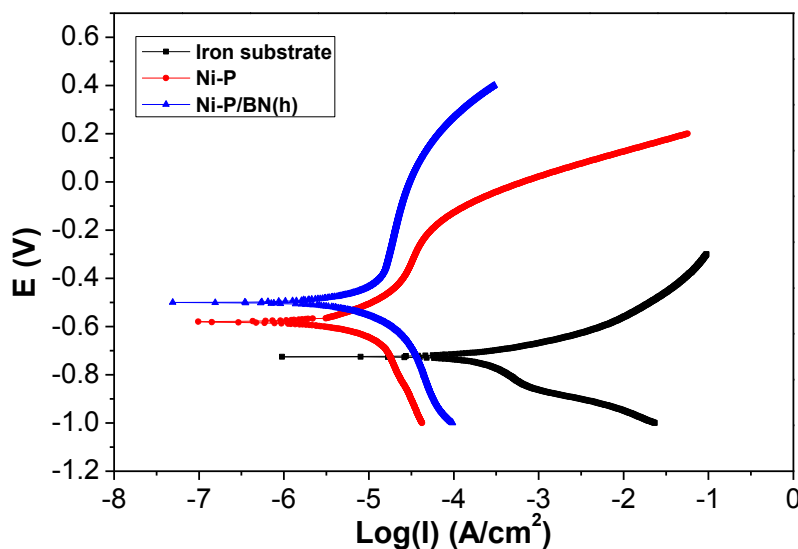


Figure 5. Potentiodynamic polarization curves of steel substrate, Ni-P coatings and Ni-P/BN(h) composite coatings in 3.5wt.% NaCl solution.

Table 4. Corrosion characteristics of iron substrate, Ni-P and Ni-P/BN(h) composite coatings in 3.5wt.% NaCl solution.

Coatings	Polarization					EIS	
	E_{corr} (V)	I_{corr} (μAcm^{-2})	B_a (mV)	B_c (mV)	R_p (Ωcm^2)	R_s (Ωcm^2)	R_c (Ωcm^2)
Iron substrate	-0.73	138.32	58.86	58.32	92	9.36	124
Ni-P	-0.58	1.75	87.08	68.53	9,528	8.72	10,582
Ni-P/BN(h)	-0.50	1.69	96.68	67.38	10,491	8.64	12,763

It can be noticed that the corrosion current of Ni-P and Ni-P/BN(h) composite coating is 1.75 μAcm^{-2} and 1.69 μAcm^{-2} respectively, representing no significant difference. However, the corrosion potential has increased from -0.58V for Ni-P coating up to -0.50V for Ni-P/BN(h) composite coating, verifying better corrosion resistance of Ni-P/BN(h) composite coating than that of Ni-P coating in 3.5 wt.% NaCl solution. In comparison to the potentiodynamic curves of Ni-P coating, the anodic dissolution reaction of Ni-P/BN(h) composite coating was restrained, which could be correlated to the reduction of the active surface due to the presence of BN(h) particles.

Adding BN(h) particles can increase the corrosion resistance of Ni–P composite coating, which can be attributed to an enhanced barrier effect caused by the presence of the BN(h) particles in the Ni–P matrix. In other words, BN(h) particles reduced Ni–P alloy matrix exposed range, thereby enhancing the corrosion resistance of composite coatings. Wang et al.[36] show that incorporation of SiC particles in an electroless Ni–P matrix can improve the corrosion behavior of electroless Ni–P coatings. Novakovic et al.[9] explore the effect of co-deposition TiO₂ particles into Ni–P matrix which also increase corrosion resistant of composite coatings.

The corrosion potential of both coatings is much more positive than iron substrate and the corrosion current density has lower about 100 times than iron substrate. According to the above conclusion that the corrosion resistance of priority order is: Ni–P/BN(h) composite coating > Ni–P coating > Iron substrate.

3.4.2. Electrochemical impedance spectroscopy (EIS)

In order to further understand the corrosion behavior of iron substrate, Ni–P and Ni–P/BN(h) composite coatings were examined by Electrochemical impedance spectroscopy(EIS).

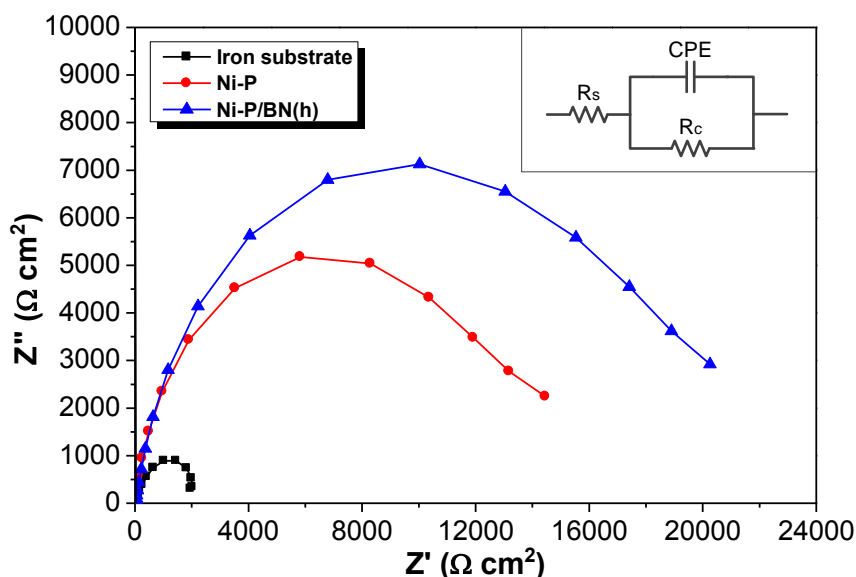


Figure 6. Nyquist plots of iron substrate, Ni–P and Ni–P/BN(h) composite coatings in the 3.5 wt.% NaCl solution.

Figure 6 shows the Nyquist plots of the iron substrate, Ni–P and Ni–P/BN(h) composite coatings. These Nyquist plots appear to be similar with respect to their shape, but the diameter of the loops are different. In other words, the capacitive loop diameters can be used to calculate the impedance value that bigger capacitive loop diameters indicate the better corrosion resistance, the results are presented in Table 4. Therefore, according to the results of EIS it shows that the corrosion resistance of Ni–P/BN(h) composite coating is the best, and the iron substrate is the worst. Measurement results from EIS show that the corrosion resistance is consistent with the polarization.

4. CONCLUSIONS

The properties of Ni–P/BN(h) composite coating has been investigated and compared with Ni–P coating and iron substrate. The results are summarized as follows:

- (1) BN(h) particles have been successfully through surfactant CTAB to uniformly co-deposited in Ni–P matrix.
- (2) The microstructure of Ni–P and Ni–P/BN(h) composite coatings are amorphous, and BN(h) particles do not change the microstructure of Ni–P coating.
- (3) BN(h) particle is an excellent solid lubricant that co-deposited with Ni–P matrix leads to decreasing hardness, while through suitable heat treatment can significantly improve the hardness of Ni–P/BN(h) composite coating.
- (4) The electrochemical and corrosion experiments prove that the addition of BN(h) particles can significantly improve corrosion resistance compared to the conventional Ni–P coating in the 3.5wt.% NaCl solution due to the presence of BN(h) particles which enhanced barrier effect in the Ni–P matrix.

References

1. R. Taheri, I. N. A. Oguocha, S. Yannacopoulos, *Wear*, 249 (2001) 389.
2. P. Sahoo, S. K. Das, *Mater. Des.*, 32 (2011) 1760.
3. J. Sudagar, J. Lian, W. Sha, *J. Alloys Compd.*, 571 (2013) 183.
4. H. Xu, Z. Yang, M. K. Li, Y. L. Shi, Y. Huang, H.-L. Li, *Surf. Coat. Technol.*, 191 (2005) 161.
5. H. Mazaheri, S. R. Allahkaram, *Appl. Surf. Sci.*, 258 (2012) 4574.
6. X. D. Yuan, X. J. Yang, *Wear*, 269 (2010) 291.
7. M. Ebrahimian-Hosseiniabadi, K. Azari-Dorcheh, S. M. Moonir Vaghefi, *Wear*, 260 (2006) 123.
8. S. M. Monir Vaghefi, A. Saatchi, M. Ebrahimian-Hoseiniabadi, *Surf. Coat. Technol.*, 168 (2003) 259.
9. J. Novakovic, P. Vassiliou, K. Samara, T. Argyropoulos, *Surf. Coat. Technol.*, 201 (2006) 895.
10. D. Dong, X. H. Chen, W. T. Xiao, G. B. Yang, P. Y. Zhang, *Appl. Surf. Sci.*, 255 (2009) 7051.
11. Y. de Hazan, D. Zimmermann, M. Z'Graggen, S. Roos, C. Aneziris, H. Bollier, P. Fehr, T. Graule, *Surf. Coat. Technol.*, 204 (2010) 3464.
12. J. N. Balaraju, V. Ezhil Selvi, K. S. Rajam, *Mater. Chem. Phys.*, 120 (2010) 546.
13. S. Alirezaei, S. M. Monirvaghefi, M. Salehi, A. Saatchi, *Wear*, 262 (2007) 978.
14. J. N. Balaraju, Kalavati, K. S. Rajam, *Surf. Coat. Technol.*, 200 (2006) 3933.
15. M. Islam, M. R. Azhar, N. Fredj, T. D. Burleigh, O. R. Oloyede, A. A. Almajid, S. Ismat Shah, *Surf. Coat. Technol.*, 261 (2015) 141.
16. H. Luo, M. Leitch, Y. Behnamian, Y. Ma, H. Zeng, J. L. Luo, *Surf. Coat. Technol.*, 277 (2015) 99.
17. T. R. Tamilarasan, R. Rajendran, G. Rajagopal, J. Sudagar, *Surf. Coat. Technol.*, 276 (2015) 320.
18. C. I. Hsu, K. H. Hou, M. D. Ger, G. L. Wang, *Appl. Surf. Sci.*, 357, Part B (2015) 1727.
19. S. Sadreddini, A. Afshar, *Appl. Surf. Sci.*, 303 (2014) 125.
20. S. Sadreddini, Z. Salehi, H. Rassaie, *Appl. Surf. Sci.*, 324 (2015) 393.
21. J. Eichler, C. Lesniak, *J. Eur. Ceram. Soc.*, 28 (2008) 1105.
22. O. A. León, M. H. Staia, H. E. Hintermann, *Surf. Coat. Technol.*, 108–109 (1998) 461.
23. O. A. León, M. H. Staia, H. E. Hintermann, *Surf. Coat. Technol.*, 120–121 (1999) 641.
24. O. A. León, M. H. Staia, H. E. Hintermann, *Surf. Coat. Technol.*, 163–164 (2003) 578.
25. O. A. León, M. H. Staia, H. E. Hintermann, *Surf. Coat. Technol.*, 200 (2005) 1825.

26. I. R. Mafi, C. Dehghanian, *Appl. Surf. Sci.*, 258 (2011) 1876.
27. S. Afroukhteh, C. Dehghanian, M. Emamy, *Appl. Surf. Sci.*, 258 (2012) 2597.
28. R. A. Shakoor, R. Kahraman, U. Waware, Y. Wang, W. Gao, *Mater. Des.*, 64 (2014) 127.
29. M. Alishahi, S. M. Monirvaghefi, A. Saatchi, S. M. Hosseini, *Appl. Surf. Sci.*, 258 (2012) 2439.
30. Y. Wu, H. Liu, B. Shen, L. Liu, W. Hu, *Tribology International*, 39 (2006) 553.
31. T. Z. Zou, J. P. Tu, S. C. Zhang, L. M. Chen, Q. Wang, L. L. Zhang, D. N. He, *Materials Science and Engineering: A*, 426 (2006) 162.
32. Z. Li, J. Wang, J. Lu, J. Meng, *Appl. Surf. Sci.*, 264 (2013) 516.
33. Y. Wu, B. Shen, L. Liu, W. Hu, *Wear*, 261 (2006) 201.
34. M. F. He, W. B. Hu, C. Zhong, J. F. Weng, B. Shen, Y. T. Wu, *Trans. Nonferrous Met. Soc. China*, 22 (2012) 2586.
35. I. Sivandipoor, F. Ashrafizadeh, *Appl. Surf. Sci.*, 263 (2012) 314.
36. H. L. Wang, L. Y. Liu, Y. Dou, W. Z. Zhang, W. F. Jiang, *Appl. Surf. Sci.*, 286 (2013) 319.

© 2016 The Authors. Published by ESG (www.electrochemsci.org). This article is an open access article distributed under the terms and conditions of the Creative Commons Attribution license (<http://creativecommons.org/licenses/by/4.0/>).